GeoHazards

MDPI

Article

Low-Cost Ambient-Vibration Monitoring of an Unstable Coastal Rock Block: Identification of the Fundamental Resonance of Kounopetra (Kefalonia, Greece) with a Force-Balance IoT Node

Ioannis Vlachos [1,*], Dionysios T. G. Katerelos [2], Markos Avlonitis [1,†], Nikos Aravantinos-Zafiris [3] and Ioannis Karydis [1,4]

[1] Department of Informatics, Ionian University, Plateia Tsirigoti 7, 49100 Corfu, Greece; karydis@ionio.gr (I.K.)
[2] Department of Audio and Visual Arts, Ionian University, 49100 Corfu, Greece; dkaterelos@ionio.gr
[3] Department of Environment, Ionian University, 29100 Zakynthos, Greece; naravadinos@ionio.gr
[4] Institute of Mechanics of Natural Hazards, University Center for Research and Innovation, Ionian University, 28200 Lixouri, Greece
* Correspondence: gvlachos@ionio.gr
† Deceased. This paper is dedicated to his memory.

Abstract

Unstable rock blocks and cliffs pose a widespread geohazard, and their mechanical state can be tracked through their ambient-vibration resonance frequencies, whose decrease anticipates progressive failure. Such monitoring is usually performed with expensive broadband instrumentation, limiting spatial and temporal coverage. Here we assess whether a low-cost, IoT-enabled node—built around a Raspberry Pi single-board computer, a 24-bit sigma-delta digitiser and a force- balance accelerometer (Geobit FBA-200)—can identify the resonance of an unstable coastal rock block at the celebrated "moving rock" of Kounopetra (Paliki peninsula, Kefalonia, Greece), a site historically renowned for visually perceptible rocking boulders. We stress that the low-amplitude 7.7 Hz structural eigenvibration characterised here is a distinct phenomenon from the historically documented ∼0.3 Hz macroscopic, quasi-rigid rocking of the boulder: the former is the ambient–vibration resonance of the fractured rock mass, the latter a large-amplitude rigid-body oscillation. Two identical nodes recorded ground acceleration simultaneously for nine hours: one on the fractured Kounopetra rock mass and one on stable ground 25 m away, used as a reference. The rock station exhibits a clear, temporally stable fundamental resonance at f_0 = 7.7 Hz ($Q \approx 50$, damping $\zeta \approx 1\%$), amplified by up to an order of magnitude relative to the reference and entirely absent from it, whereas a narrow 20.5 Hz line present on both nodes is identified as instrument-related and discarded. A simultaneous two-station analysis further shows that the ambient sources are extremely local (only 0.4% of transient activity is common to the two nodes 25 m apart), quantifying a design constraint for differential schemes. The results demonstrate that a low-cost force-balance node is sufficient to establish a resonance baseline for an unstable rock block, opening the way to dense, affordable early-warning networks; the main limitations are the single vertical component and the short record, which preclude polarisation analysis and long-term tracking of f_0.

Keywords: unstable rock slope; ambient vibration; resonance frequency; low-cost seismograph; force-balance accelerometer; rockfall early warning; Kounopetra; Kefalonia

Check for updates

Academic Editor: Yuchen Wang

Received: 28 July 2026
Revised: 14 August 2026
Accepted: 17 August 2026
Published: 19 August 2026

Copyright: © 2026 by the authors. Licensee MDPI, Basel, Switzerland. This article is an open access article distributed under the terms and conditions of the Creative Commons Attribution (CC BY) license.

1. Introduction

Rockfalls and the collapse of unstable rock blocks and cliffs are among the most widespread and rapid geohazards, threatening coastal roads, settlements and cultural sites worldwide. A physically grounded and increasingly established way to assess the stability of a rock compartment is to monitor its ambient–vibration response: a partially detached rock mass behaves as a mechanical oscillator with its own eigenfrequencies, which are excited by the omnipresent ambient seismic noise and can be recovered without any active source [1,2].

The approach has been applied to a broad range of unstable structures, from prone-to-fall rock columns and natural rock arches to large unstable slopes, using both spectral and microseismic methods [3–6]. Crucially, the fundamental resonance frequency f_0 is a proxy for the mechanical integrity of the compartment: as the rock bridges that connect the block to the stable massif progressively fracture, the effective stiffness drops and f_0 decreases, so that a measured decline of f_0 provides an early, quantitative warning of impending failure [3,7], in direct analogy with the loss of stiffness that lowers the natural frequencies of a damaged engineered structure [8]. This resonance-based approach complements the broader geophysical toolbox used for landslide and rockfall early-warning systems [9–12]; in practice, the damage-driven decrease in f_0 must be separated from its reversible, temperature-driven modulation [13], an issue we return to in Section 5.

The resonance of an unstable compartment is most simply revealed by comparing its ambient–vibration spectrum with that of a nearby station on stable ground: the ratio isolates the site/structure response and produces a peak at the block's eigenfrequency, in the same spirit as the horizontal-to-vertical spectral-ratio technique used for soil site characterisation [1,14] and increasingly adapted to the ambient-noise response of landslide-prone slopes [15]. To date, such measurements have relied on research-grade broadband seismometers, which are expensive, power-hungry and logistically demanding; this restricts monitoring to a few high-value sites and to short campaigns rather than the continuous, spatially dense observation that early warning requires.

In parallel, low-cost single-board computers, micro-electromechanical and force-balance sensors and cellular connectivity have made it possible to build autonomous seismic nodes at a cost one to two orders of magnitude lower than that of professional stations [16,17], and such nodes have already been used to monitor rockfalls and slope processes in the field [18,19]. Their noise floor is, however, higher and site-dependent, and it is not obvious that such hardware can resolve the subtle ambient resonance of a rock block. This paper addresses that question directly at an emblematic site.

Motivation and Contributions

Motivation. Kounopetra, on the Paliki peninsula of Kefalonia (Ionian Sea, Greece), is a celebrated site renowned for visually perceptible "moving rocks": slow rhythmic rocking motions have been reported there for successive coastal boulders over many decades. The historically famous Kounopetra boulder ceased rocking after the $M_s \approx 7.2$ 1953 Ionian earthquake [20]; according to local accounts, a similar motion was subsequently reported on a neighbouring block—the fractured rock investigated here. The site therefore combines a genuinely fractured, partially detached rock geometry with strong public and scientific interest, making it an ideal, well-motivated testbed for low-cost resonance monitoring in the most seismically active region of Greece.

Contributions. The specific contributions of this paper are:

1. A low-cost, IoT-enabled force-balance node (Raspberry Pi, 24-bit sigma-delta digitiser, Geobit FBA-200 accelerometer) deployed for ambient–vibration monitoring of an unstable coastal rock;

2. The identification of the fundamental resonance of the Kounopetra rock at $f_0 = 7.7$ Hz ($Q \approx 50$), amplified relative to and absent from a stable reference 25 m away, with an explicit rejection of an instrument-related spectral line;
3. A real, simultaneous two-station measurement quantifying how local the ambient sources are (common-mode fraction $\approx 0.4\%$ at 25 m), which constrains the geometry of differential detection schemes; and
4. An honest assessment of what a single-vertical-component, short-duration low-cost record can and cannot establish, as a basis for long-term early-warning deployments.

The remainder of this paper is organised as follows. Section 2 describes the Kounopetra site and its history. Section 3 presents the instrumentation, the field deployment and the ambient–vibration analysis. Section 4 reports the noise characterisation, the resonance identification and its validation. Section 5 discusses the implications for early warning and the study limitations, and Section 6 concludes.

2. Study Area: The "Moving Rock" of Kounopetra

Kounopetra ("the rock that rocks") lies at the southern tip of the Paliki peninsula, south of the village of Mantzavinata in southwestern Kefalonia, Ionian Sea. It consists of a low, heavily fractured coastal rock platform that juts into the sea and is segmented, by open fissures, into a set of metre-scale, partially detached blocks (Figure 1a,c). The wider region sits at the northern end of the Cephalonia Transform Fault Zone, a major dextral strike-slip boundary and one of the most seismically active structures in the Mediterranean [21,22], which has repeatedly produced strong ($M_w > 6$) earthquakes, including the 2014 Kefalonia doublet [23]. This persistent regional seismicity both supplies the ambient wavefield that excites the rock's resonance and constitutes the principal external trigger against which its stability must be monitored [20].

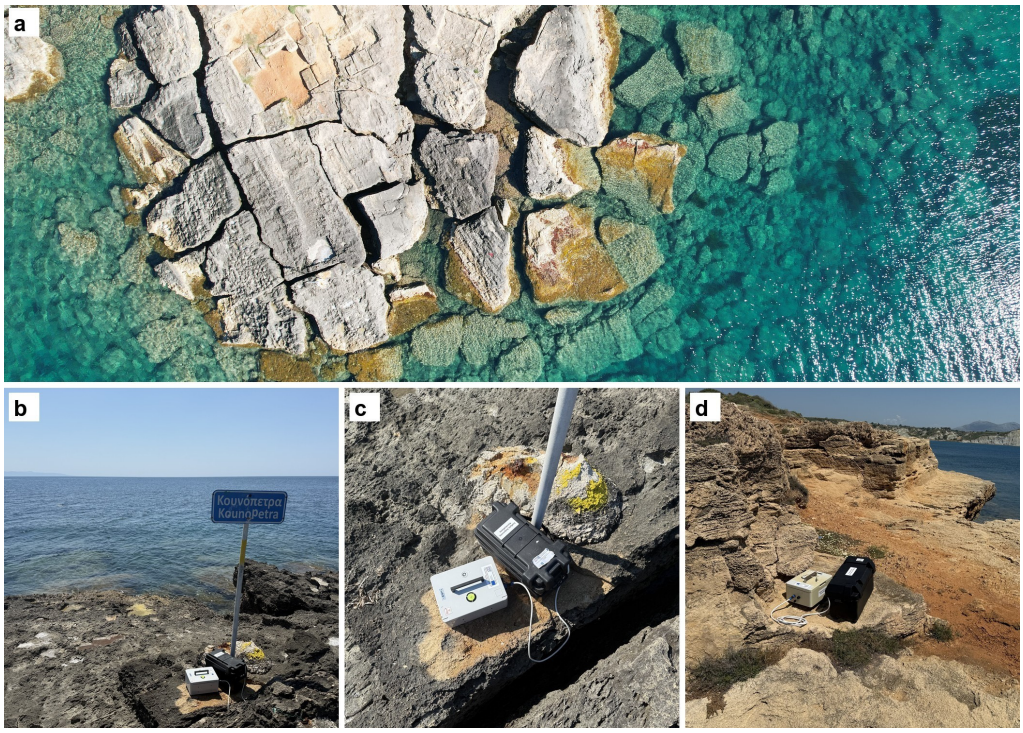


Figure 1. Field site at Kounopetra, Kefalonia: (**a**) top-down aerial view of the fractured rock platform; (**b**) the rock node at the "Kounopetra" sign; (**c**) close-up of the node beside an open fissure; (**d**) the reference node on stable ground.

Historically, the Kounopetra coastal area has been renowned for the occurrence of visually perceptible rocking boulders. Along this section of the shoreline, sandstone formations are continuously eroded by marine processes, progressively creating an unstable foundation beneath the overlying rock blocks. As a result, slow rhythmic rocking motions have been reported for different boulders within the area over many decades.

Historical accounts describe oscillations of approximately twenty cycles per minute (∼0.3 Hz), which could be observed from the shore and reportedly felt as a pulsation when standing on the moving rock. Following the 12 August 1953 Ionian earthquake ($M_s \approx 7.2$), which caused widespread coastal uplift and significant geomorphological changes across Kefalonia [20], the conspicuous rocking motion of the historically known Kounopetra boulder ceased. Subsequently, however, and according to local historical accounts, a similar visually perceptible rocking motion was reported on a neighbouring boulder—the rock investigated in the present study. This relocation of the phenomenon is consistent with the interpretation that the visible rocking motion is controlled by local geological and geomorphological conditions rather than being an intrinsic property of a particular rock. In particular, the progressive erosion of the underlying sandstone formations may create unstable support conditions for individual rock blocks, while major earthquakes may sufficiently modify these conditions to suppress the rocking of one block and promote similar behaviour in another nearby block.

We stress that this historically documented ∼0.3 Hz macroscopic rocking motion is distinct from the ∼7.7 Hz structural resonance characterised in the present study. The former corresponds to a large-amplitude, quasi-rigid oscillation of a rock block, whereas the latter represents the low-amplitude eigenvibration of the fractured rock mass excited by ambient vibrations. The objective of the present study is therefore not to reconstruct the historical rocking phenomenon, but to establish, using low-cost instrumentation, are producible modern baseline of the resonant state of the investigated rock block.

3. Materials and Methods

3.1. Low-Cost Force-Balance Node

Each monitoring node integrates a Raspberry Pi single-board computer (Raspberry Pi Ltd., Cambridge, UK), a Waveshare ADS1256 24-bit sigma-delta analogue-to-digital converter (Waveshare Electronics, Shenzhen, China), and a Geobit FBA-200 force-balance (servo) accelerometer (GEObit Instruments, Patras, Greece) sensing the vertical ground acceleration component, housed in an IP66 weatherproof enclosure with solar power and a 4G/LTE modem for one-minute data upload (Figure 2). This architecture follows the low-latency, low-cost embedded force-balance accelerograph line of development for early-warning applications [19,24], with the force-balance sensor providing the sensitivity and dynamic range required for ambient–vibration work while keeping the per-node cost low. A single vertical component was a deliberate design choice: it halves the sensor and acquisition cost relative to a three-component node and minimises power, while the vertical ground motion expresses the ambient–vibration resonance of a coastal rock block clearly enough to identify and track f_0 robustly. Resolving the direction of the resonant motion (translational versus rocking modes) would instead require a three-component sensor and is left to future work.

The accelerometer was operated at a programmable-gain-amplifier setting of unity (PGA = 1) over a ±2 g range; with a 24-bit conversion this yields a quantisation step of $4\ \mathrm{g}/2^{24} \approx 0.24\ \mu\mathrm{g}$, far below the ambient ground noise, so that the records are never digitiser-limited. Data are acquired continuously at a nominal rate of ∼100 Hz; the effective rate measured from the sample timestamps is 96.95 Hz (Nyquist frequency 48.5 Hz), which

comfortably covers the sub-30 Hz band relevant to rock-block resonances. Each one-minute file contains the vertical acceleration in units of g together with a high-resolution timestamp.

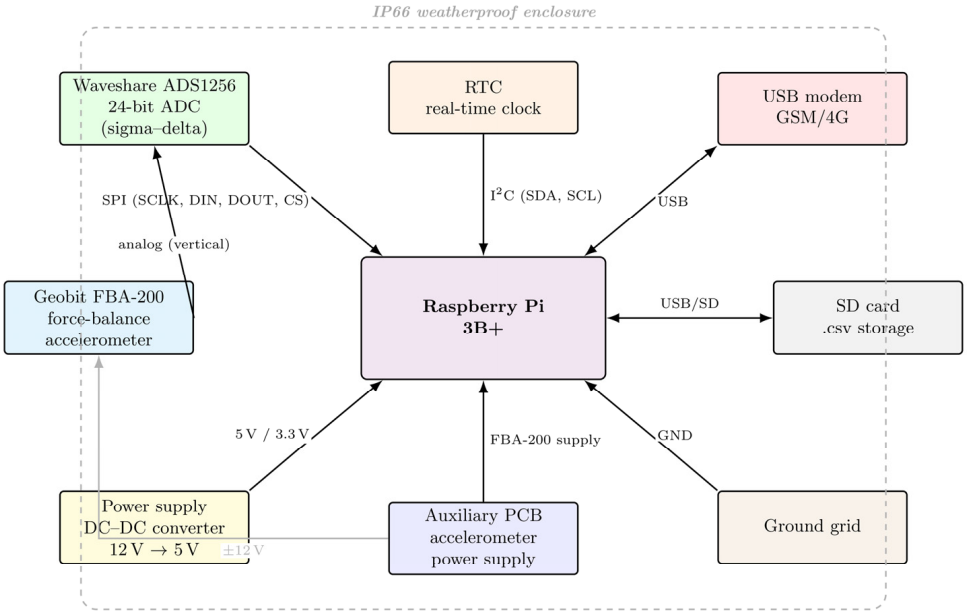


Figure 2. Block diagram of the low-cost force-balance monitoring node inside its IP66 weatherproof enclosure.

The block diagram of Figure 2 summarises the full acquisition and telemetry workflow. The vertical output of the FBA-200 servo accelerometer (GEObit Instruments, Patras, Greece) is fed directly to the differential input of the ADS1256 converter (Texas Instruments, Dallas, TX, USA), whose on-chip programmable-gain amplifier and 24-bit conversion supply the required sensitivity and dynamic range without an external preamplifier; the digitiser streams samples to the Raspberry Pi over the SPI bus at the nominal ∼100 Hz rate. Each sample is tagged on the Pi with a high-resolution timestamp, and the Pi clock is disciplined over the network (NTP) through the 4G/LTE link, so that the independent nodes share a common absolute time to sub-second accuracy—the property exploited by the two-station analysis below. Samples are buffered locally and written to consecutive one-minute files, which are transmitted over the 4G/LTE modem to the server; this bounds any loss during a connectivity outage to a single file while keeping the data available in near-real time. The whole chain operates off-grid: a photovoltaic panel and charge controller maintain a battery that supplies regulated power to the single-board computer, the analogue front-end and the modem, enabling continuous unattended operation.

3.2. Field Deployment

Two identical nodes were deployed at Kounopetra on 2 May 2025 and recorded simultaneously for approximately nine hours (11:00–20:00 local time). One node (the rock station) was installed directly on the fractured Kounopetra rock mass, next to the "Kounopetra" landmark sign and adjacent to an open fissure that bounds the instrumented block (Figure 1b,c). The second node (the reference station) was placed on stable ground on softer sedimentary substrate about 25 m away (Figure 1d). The two nodes are hardware-identical and were configured identically, so that any systematic spectral difference between them reflects the ground/structure and not the instrument.

The deployment geometry is summarised schematically in Figure 3: the rock station S_{rock} sits on the fractured Kounopetra block, where the resonance is expected, while the

reference station S_{ref} occupies stable ground about 25 m away, a separation at which—as shown below—the two nodes share almost none of their local ambient sources.

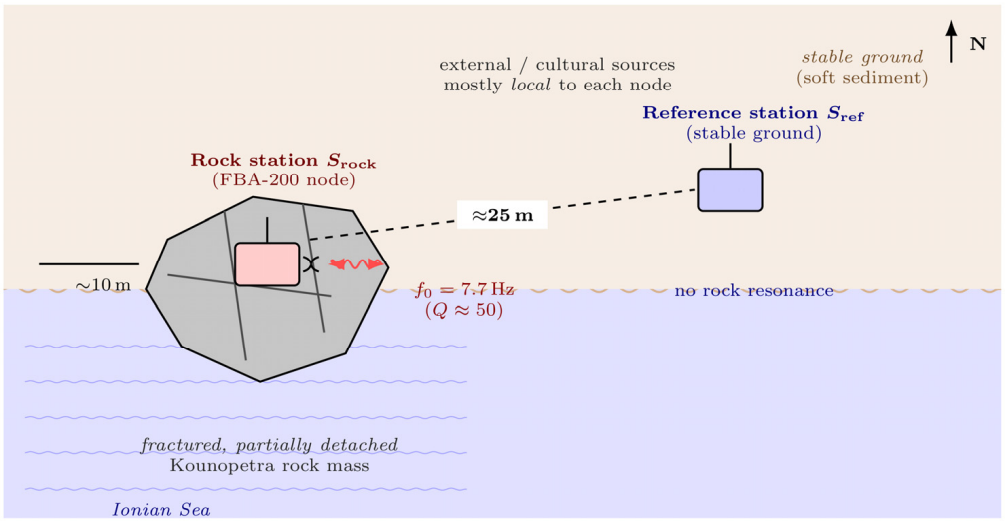


Figure 3. Schematic plan view of the two-station field deployment at Kounopetra: rock station S_{rock} on the fractured rock mass and reference station S_{ref} on stable ground ≈ 25 m away.

3.3. Ambient–Vibration Analysis

For each node the continuous vertical-acceleration record was detrended (mean removal) and, where a broadband noise floor was required, high-pass filtered above 0.5 Hz. Power spectral densities (PSDs) were estimated with Welch's method on consecutive five-minute blocks (Hann window, 16,384-sample segments) and the median across blocks was taken, which is robust to the transient cultural bursts present in the records. The rock resonance is characterised by the spectral ratio

$$R(f) = \sqrt{\frac{S_{rock}(f)}{S_{ref}(f)}} \tag{1}$$

where $R(f)$ is the square root of the ratio of the median PSDs of the rock and reference stations, which peaks at the block's eigenfrequencies while suppressing sources common to both sites [1,14]. For each resonance the fundamental frequency f_0, the half-power bandwidth Δf and the quality factor $Q = f_0/\Delta f$ (with equivalent viscous damping $\zeta = 1/(2Q)$) were estimated. The temporal stability of f_0 was assessed by tracking the spectral peak in one-minute windows over the whole record, and its persistence was verified on the time-frequency spectrogram. Candidate resonances were tested against artificial (instrument or machine) origins by checking whether the line (i) appears on the reference node as well, and (ii) is anomalously narrow; a line common to both identical nodes and of very high Q was attributed to the instrumentation and discarded. Finally, transient activity at the two stations was compared second-by-second to quantify the fraction of ambient sources common to both sites.

4. Results

4.1. Instrument Noise and Data Quality

Over the nine-hour common window the two nodes acquired ~3.1 million samples each at a stable 96.95 Hz. Both records are dominated by real ground and cultural vibration rather than by digitiser noise: the quietest one-minute ambient level on the reference node is of order 10^2 µg root-mean-square, i.e., several hundred times the 0.24 µg quantisation step, confirming that the low-cost acquisition chain resolves the ambient wavefield with ample

margin. The two sites nonetheless differ markedly in their spectral character (Figure 4a): the reference station shows a smooth, monotonically decaying ambient spectrum typical of a soft-ground site, whereas the rock station superimposes on a lower broadband level a set of discrete spectral peaks.

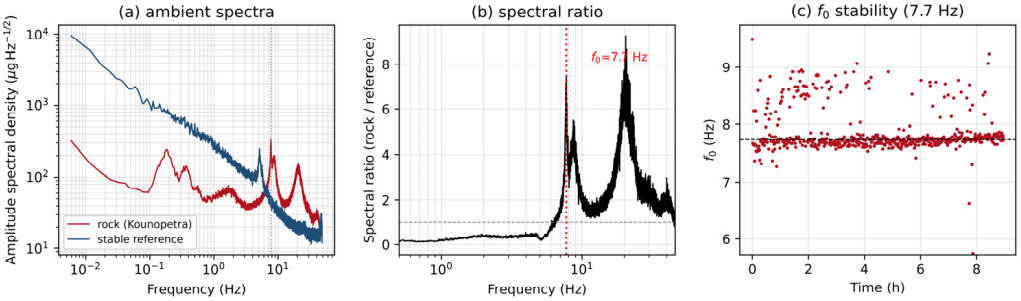


Figure 4. Modal characterisation of the Kounopetra rock: (**a**) median ambient amplitude spectral density of the rock and the stable reference; (**b**) rock/reference spectral ratio; (**c**) minute-by-minute tracking of f_0.

4.2. Fundamental Resonance of the Rock

The spectral ratio between the rock and the reference (Equation (1)) reveals a clear, dominant resonance at $f_0 = 7.7$ Hz (Figure 4b), amplified by roughly an order of magnitude (a factor of ∼8–12) relative to the stable reference and entirely absent from the reference spectrum. A modal fit of the peak yields a quality factor $Q \approx 50$, corresponding to an equivalent viscous damping of $\zeta \approx 1\%$, values consistent with the lightly damped, partially coupled resonance of a fractured rock compartment [2,7].

The resonance is temporally stable: tracking the spectral peak minute-by-minute over the whole record gives a median $f_0 = 7.7$ Hz with a scatter of only 0.37 Hz (4.8%; Figure 4c). The underlying minimal dataset—the median ambient spectra, the rock/reference spectral ratio, and the minute-by-minute f0 series shown in Figure 4—is provided in Supplementary File S1.

On the time-frequency spectrogram of the rock station (Figure 5) the resonance appears as a continuous horizontal band at ∼7.7 Hz that persists throughout the nine hours, superimposed on vertical stripes that correspond to local transient (cultural) events; the band is absent from the reference station, as already shown by the spectral ratio (Figure 4). The permanence of the line, and the modulation of its amplitude by the ambient noise level, are the expected signature of a structural resonance excited by ambient vibration rather than of an active source.

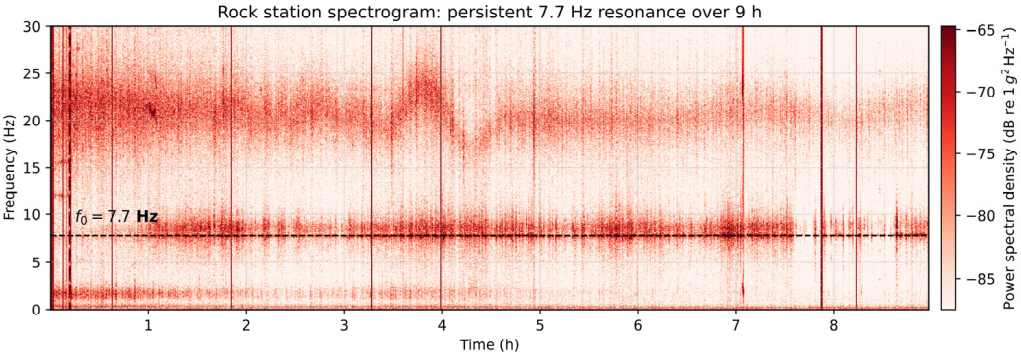


Figure 5. Time-frequency spectrogram of the rock station (white = low and red = high power spectral density). The persistent red band at $f_0 = 7.7$ Hz (dashed line) is the rock resonance.

4.3. Rejection of an Instrument-Related Line

A narrow spectral line near 20.5 Hz is also present in the rock record. High-resolution frequency analysis, however, shows that this line appears on both the rock and the reference nodes and is extremely narrow (quality factor of several hundred to over one thousand), in contrast to the 7.7 Hz resonance which is confined to the rock and has a moderate $Q \approx 50$. A very high Q line common to two identical, co-configured nodes is the signature of an internal, instrument-related source (e.g., a switching or clock tone of the shared electronics) rather than of a ground resonance; accordingly, the 20.5 Hz line is attributed to the instrumentation and is not interpreted as a structural mode. Three further observations support this attribution: the line sits at the same nominal frequency on the two independent nodes yet carries no cross-station coherence (Section 4.4), indicating that each node generates it internally rather than sharing an external source; its quality factor is one to two orders of magnitude higher than that of any documented rock-block or site resonance; and, unlike the 7.7 Hz peak, it is not amplified on the rock relative to the reference. This check illustrates the importance, in low-cost deployments, of distinguishing genuine ground resonances from hardware artefacts by exploiting the presence of an identical reference node.

4.4. Locality of the Ambient Sources

Because the two nodes recorded simultaneously—at the same effective sampling rate (96.95 Hz) and with clocks that agree to within 0.1 s, both records terminating at the same scheduled wall-clock time—the sharing of the ambient field between them can be measured directly. We quantify it in the time domain, by comparing transient activity second-by-second, rather than through a magnitude-squared coherence spectrum: the two nodes are independently NTP-disciplined and are not synchronised at the sample (millisecond) level, so a cross-station coherence is dominated by the residual timing offset above a few hertz and is not a reliable measure of common sources; the one-second bins of the transient metric, in contrast, are robust to that sub-second offset.

Comparing transient seconds (root-mean-square exceeding five times the median) band by band, the fraction common to both stations is low across the entire spectrum (Figure 6): it is highest at low frequency (3.9% in the 1–3 Hz band, where long-wavelength regional and microseismic sources are more likely to be shared) and falls below 1% over most of the band, including $\approx 1\%$ in the 6–10 Hz band that contains the resonance. Pooled over 1–20 Hz, only $\approx 0.4\%$ of transient seconds are common to both stations, and the ten strongest transients of each node are essentially invisible ($\sim$1% relative amplitude) at the other node 25 m away; the envelope correlation between the two stations is statistically null. The ambient and cultural sources are therefore extremely local at the scale of 25 m, and in particular the 7.7 Hz activity is not a shared ambient source. This has a direct design implication for differential (reference-based) detection schemes: a reference station intended to reject common external sources must be placed much closer than 25 m to share those sources, otherwise it rejects almost nothing. In practical terms, at a 25 m separation the reference is effectively an independent control rather than a common-mode canceller: it cannot subtract shared external noise, but it does establish that a spectral peak seen only on the rock is site-specific—precisely the role it plays here in confirming the 7.7 Hz resonance and in exposing the 20.5 Hz instrument line. Effective common-mode rejection for a differential early-warning scheme would instead require co-locating the reference within a few metres of the monitored block, whereas a control station to verify that a detected resonance is genuine can be placed freely at tens of metres.

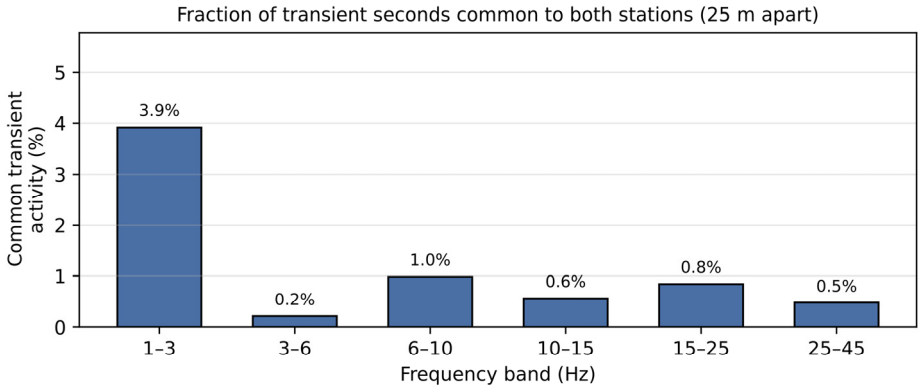


Figure 6. Fraction of transient seconds (RMS > 5× median) common to the rock and reference stations 25 m apart, resolved by frequency band. The shared fraction is low throughout (≤4%), highest at low frequency and only ≈ 1% in the 6 –10 Hz resonance band, confirming that the ambient sources—and the 7.7 Hz resonance in particular—are local to each node. A magnitude-squared coherence spectrum is not used because the two independently clocked nodes are not synchronised at the sample level (see text).

5. Discussion

The measurements show that a low-cost, IoT-enabled force-balance node can identify and characterise the fundamental resonance of an unstable rock block. The 7.7 Hz resonance of Kounopetra is well defined (Q ≈ 50), strongly amplified with respect to the reference, temporally stable, and confined to the fractured rock mass—all consistent with the eigenvibration of a partially detached compartment as documented for larger unstable slopes with research-grade instrumentation [1–3,7]. The fractured, block-segmented geometry visible in the aerial imagery (Figure 1a) provides an independent geological basis for the existence of such a mode. The platform is a heavily fractured Pleistocene coastal sandstone (Section 2) whose open fissures delimit the metre-scale, partially detached block that was instrumented. A quantitative geomechanical characterisation—in situ mapping of the fracture geometry and rock-bridge dimensions, and laboratory determination of the density and elastic moduli of the sandstone—would allow the measured f_0 to be matched to a theoretical stiffness through Equation (2); such field and laboratory work was beyond the scope of the present low-cost feasibility study and is a natural next step.

The practical value of this result lies in monitoring. To first order the compartment behaves as a single-degree-of-freedom oscillator, so that

$$f_0 = \frac{1}{2\pi}\sqrt{\frac{k_{eff}}{m}}, \tag{2}$$

where m is the effective mass of the block and k_{eff} the effective stiffness of the rock bridges that connect it to the stable massif. Because m is essentially constant, the progressive fracturing that precedes failure reduces k_{eff} and therefore lowers f_0 (Equation (2)); a continuous, low-cost record of f_0 thus constitutes a physically based early-warning observable. The 7.7 Hz value reported here is a baseline: a stable low-cost node left in place over seasons to years would allow the detection of any secular decrease, or of transient drops following strong regional earthquakes such as those repeatedly generated by the adjacent Cephalonia Transform Fault. The affordability of the node makes it realistic to instrument many such compartments simultaneously.

Several limitations must be stated honestly. First, the node records a single vertical component; the identification of f_0 is robust, but the direction of the resonant motion, and hence a full modal (polarisation) analysis of the block, cannot be obtained and would

require a three-component sensor [1]. Second, the record is only nine hours long, which is sufficient to establish and validate the resonance but not to observe the seasonal or damage-induced evolution of f_0 on which early warning ultimately depends. Turning the static baseline reported here into a functional warning workflow will require continuous, multi-season operation—on the order of at least six months and ideally spanning post-seismic intervals—so that the reversible, diurnal-to-seasonal modulation of f_0 driven by temperature and other environmental forcing (of the order of a few percent for comparable rock compartments [13]) can be characterised and removed to isolate any irreversible, damage-driven decrease. Because the present node did not log temperature or other environmental variables alongside the acceleration, such a separation could not be attempted here; co-locating temperature, humidity and, ideally, tidal and wind sensors with the accelerometer is a specific requirement for the long-term deployments that a warning system would need. Third, the fundamental at 7.7 Hz is characterised here; the higher modes were either weak or, in the case of the 20.5 Hz line, of instrumental origin, so that only the fundamental is tracked. Finally, the value of f_0 depends on the specific instrumented block; extending the survey to neighbouring compartments would map the spatial variability of the resonance across the Kounopetra platform.

6. Conclusions

We have shown that a low-cost, solar-powered IoT node built from a Raspberry Pi, a 24-bit sigma-delta digitiser and a Geobit FBA-200 force-balance accelerometer can identify the fundamental ambient–vibration resonance of an unstable coastal rock block. What this nine-hour campaign experimentally demonstrates is specific and bounded: at the emblematic "moving rock" of Kounopetra, Kefalonia, the node resolves a clear resonance at f_0 = 7.7 Hz ($Q \approx 50$, damping $\approx$ 1%) that is temporally stable over the recording window (Figure 4c), amplified by up to an order of magnitude relative to, and absent from, a stable reference station 25 m away; a spurious 20.5 Hz line common to both identical nodes is identified as instrument-related and rejected; and a simultaneous two-station analysis quantifies the strong locality of the ambient field (≈0.4% common-mode at 25 m), which constrains the geometry of reference-based detection. Together these establish a reproducible resonance baseline and show that affordable force-balance nodes are metrologically adequate for the ambient–vibration characterisation of unstable rock compartments.

We equally stress what has not been demonstrated here. A nine-hour, single-vertical-component record cannot establish the long-term behaviour of f_0, separate its reversible thermal modulation from an irreversible, damage-driven decrease, or resolve the polarisation of the resonant motion; it therefore does not by itself constitute an early-warning system, but rather the validated first step towards one. Turning the demonstrated baseline into an operational early-warning network will require three-component nodes for modal analysis and continuous, multi-season deployments—co-located with environmental sensors—to track the evolution of f_0. The affordability demonstrated here is precisely what makes such dense, long-term networks realistic.

Supplementary Materials: The following supporting information can be downloaded at: https://www.mdpi.com/article/10.3390/geohazards7030101/s1, Supplementary File S1: minimal dataset: median ambient spectra, spectral ratio, and f0 tracking.

Author Contributions: Conceptualisation, I.V. and M.A.; methodology, I.V., D.T.G.K. and M.A.; software, I.V.; validation, I.V., N.A.-Z. and D.T.G.K.; formal analysis, I.V. and D.T.G.K.; investigation, I.V. and N.A.-Z.; data curation, I.V. and N.A.-Z.; writing—original draft, I.V.; writing—review and editing, I.V., N.A.-Z., D.T.G.K. and I.K.; supervision, M.A. and I.K. Author M.A. passed away prior to

the publication of this manuscript. All other authors have read and agreed to the published version of this manuscript.

Funding: This research received no external funding.

Data Availability Statement: The original contributions presented in this study are included in the article and Supplementary Material. Further inquiries can be directed to the corresponding authors.

Acknowledgments: The authors gratefully thank Panagis Trompetas for the substantial technical support he provided in carrying out the field experiment. This work is dedicated to the memory of our beloved colleague and co-author, the Markos Avlonitis, and to his family; his vision for low-cost, accessible instrumentation inspired this research. During the preparation of this manuscript, the authors used a generative-AI large language model to assist with language editing and with the generation of figure and data-analysis code; all data, analyses, interpretation and conclusions were produced and verified by the authors, who take full responsibility for the content of this work.

Conflicts of Interest: The authors declare no conflicts of interest.

References

1. Burjánek, J.; Gassner-Stamm, G.; Poggi, V.; Moore, J.R.; Fäh, D. Ambient vibration analysis of an unstable mountain slope. *Geophys. J. Int.* **2010**, *180*, 820–828. [CrossRef]
2. Moore, J.R.; Gischig, V.; Burjánek, J.; Loew, S.; Fäh, D. Site effects in unstable rock slopes: Dynamic behavior of the Randa instability (Switzerland). *Bull. Seismol. Soc. Am.* **2011**, *101*, 3110–3116. [CrossRef]
3. Lévy, C.; Jongmans, D.; Baillet, L. Analysis of seismic signals recorded on a prone-to-fall rock column (Vercors massif, French Alps). *Geophys. J. Int.* **2011**, *186*, 296–310. [CrossRef]
4. Starr, A.M.; Moore, J.R.; Thorne, M.S. Ambient resonance of Mesa Arch, Canyonlands National Park, Utah. *Geophys. Res. Lett.* **2015**, *42*, 6696–6702. [CrossRef]
5. Colombero, C.; Comina, C.; Vinciguerra, S.; Benson, P.M. Microseismicity of an unstable rock mass: From field monitoring to laboratory testing. *J. Geophys. Res. Solid Earth* **2018**, *123*, 1673–1693. [CrossRef]
6. Colombero, C.; Baillet, L.; Comina, C.; Jongmans, D.; Larose, E.; Valentin, J.; Vinciguerra, S. Integration of ambient seismic noise monitoring, displacement and meteorological measurements to infer the temperature- controlled long-term evolution of a complex prone-to-fall cliff. *Geophys. J. Int.* **2018**, *213*, 1876–1897. [CrossRef]
7. Kleinbrod, U.; Burjánek, J.; Hugentobler, M.; Amann, F.; Fäh, D. A comparative study on seismic response of two unstable rock slopes within same tectonic setting but different activity level. *Geophys. J. Int.* **2017**, *211*, 1428–1448. [CrossRef]
8. Clinton, J.F.; Bradford, S.C.; Heaton, T.H.; Favela, J. The observed wander of the natural frequencies in a structure. *Bull. Seismol. Soc. Am.* **2006**, *96*, 237–257. [CrossRef]
9. Whiteley, J.S.; Chambers, J.E.; Uhlemann, S.; Wilkinson, P.B.; Kendall, J.M. Geophysical monitoring of moisture-induced landslides: A review. *Rev. Geophys.* **2019**, *57*, 106–145. [CrossRef]
10. Intrieri, E.; Gigli, G.; Mugnai, F.; Fanti, R.; Casagli, N. Design and implementation of a landslide early warning system. *Eng. Geol.* **2012**, *147–148*, 124–136. [CrossRef]
11. Sättele, M.; Bründl, M.; Straub, D. Reliability and effectiveness of early warning systems for natural hazards: Concept and application to debris flow warning. *Reliab. Eng. Syst. Saf.* **2015**, *142*, 192–202. [CrossRef]
12. Michoud, C.; Bazin, S.; Blikra, L.H.; Derron, M.-H.; Jaboyedoff, M. Experiences from site-specific landslide early warning systems. *Nat. Hazards Earth Syst. Sci.* **2013**, *13*, 2659–2673. [CrossRef]
13. Bottelin, P.; Lévy, C.; Baillet, L.; Jongmans, D.; Guéguen, P. Modal and thermal analysis of Les Arches unstable rock column (Vercors massif, French Alps). *Geophys. J. Int.* **2013**, *194*, 849–858. [CrossRef]
14. Haghshenas, E.; Bard, P.-Y.; Theodulidis, N. Empirical evaluation of microtremor H/V spectral ratio. *Bull. Earthq. Eng.* **2008**, *6*, 75–108. [CrossRef]
15. Del Gaudio, V.; Muscillo, S.; Wasowski, J. What we can learn about slope response to earthquakes from ambient noise analysis: An overview. *Eng. Geol.* **2014**, *182*, 182–200. [CrossRef]
16. Cochran, E.S.; Lawrence, J.F.; Christensen, C.; Jakka, R.S. The Quake-Catcher Network: Citizen science expanding seismic horizons. *Seismol. Res. Lett.* **2009**, *80*, 26–30. [CrossRef]
17. Anthony, R.E.; Ringler, A.T.; Wilson, D.C.; Wolin, E. Do low-cost seismographs perform well enough for your network? An overview of laboratory tests and field observations of the OSOP Raspberry Shake 4D. *Seismol. Res. Lett.* **2019**, *90*, 219–228. [CrossRef]

18. Manconi, A.; Coviello, V.; Galletti, M.; Seifert, R. Short communication: Monitoring rockfalls with the Raspberry Shake. *Earth Surf. Dyn.* **2018**, *6*, 1219–1227. [CrossRef]
19. Germenis, N.; Fountas, P.; Koulamas, C. Low latency and low cost smart embedded seismo-graph for early warning IoT applications. In Proceedings of the 2020 9th Mediterranean Conference on Embedded Computing (MECO), Budva, Montenegro, 11–14 June 2020; pp. 1–4. [CrossRef]
20. Stiros, S.C.; Pirazzoli, P.A.; Laborel, J.; Laborel-Deguen, F. The 1953 earthquake in Cephalonia (Western Hellenic Arc): Coastal uplift and halotectonic faulting. *Geophys. J. Int.* **1994**, *117*, 834–849. [CrossRef]
21. Louvari, E.; Kiratzi, A.A.; Papazachos, B.C. The Cephalonia Transform Fault and its extension to western Lefkada Island (Greece). *Tectonophysics* **1999**, *308*, 223–236. [CrossRef]
22. Sachpazi, M.; Hirn, A.; Clement, C.; Haslinger, F.; Laigle, M.; Kissling, E.; Charvis, P.; Hello, Y.; Lepine, J.-C.; Sapin, M.; et al. Western Hellenic subduction and Cephalonia Transform: Local earthquakes and plate transport and strain. *Tectonophysics* **2000**, *319*, 301–319. [CrossRef]
23. Karakostas, V.; Papadimitriou, E.; Mesimeri, M.; Gkarlaouni, C.; Paradisopoulou, P. The 2014 Kefalonia doublet (Mw6.1 and Mw6.0), central Ionian Islands, Greece: Seismotectonic implications along the Kefalonia Transform Fault Zone. *Acta Geophys.* **2015**, *63*, 1–16. [CrossRef]
24. Germenis, N. A new low latency and low-cost force-balance accelerograph for earthquake and structural monitoring and for early-warning applications. In Proceedings of the EGU General Assembly 2024, Vienna, Austria, 14–19 April 2024; p. EGU24-5299. [CrossRef]

Disclaimer/Publisher's Note: The statements, opinions and data contained in all publications are solely those of the individual author(s) and contributor(s) and not of MDPI and/or the editor(s). MDPI and/or the editor(s) disclaim responsibility for any injury to people or property resulting from any ideas, methods, instructions or products referred to in the content.